The gravitational wave signature of 'realistic' 3D core collapse simulations

Simon Scheidegger

Collaborators: R. Käppeli, S.C. Whitehouse, T. Fischer, M. Liebendörfer

Outline

I. Motivation

II. Introduction to Gravitational waves

III. Modelling 3D MHD core collapse supernovae

IV. The GW signature of MHD core collapse simulations

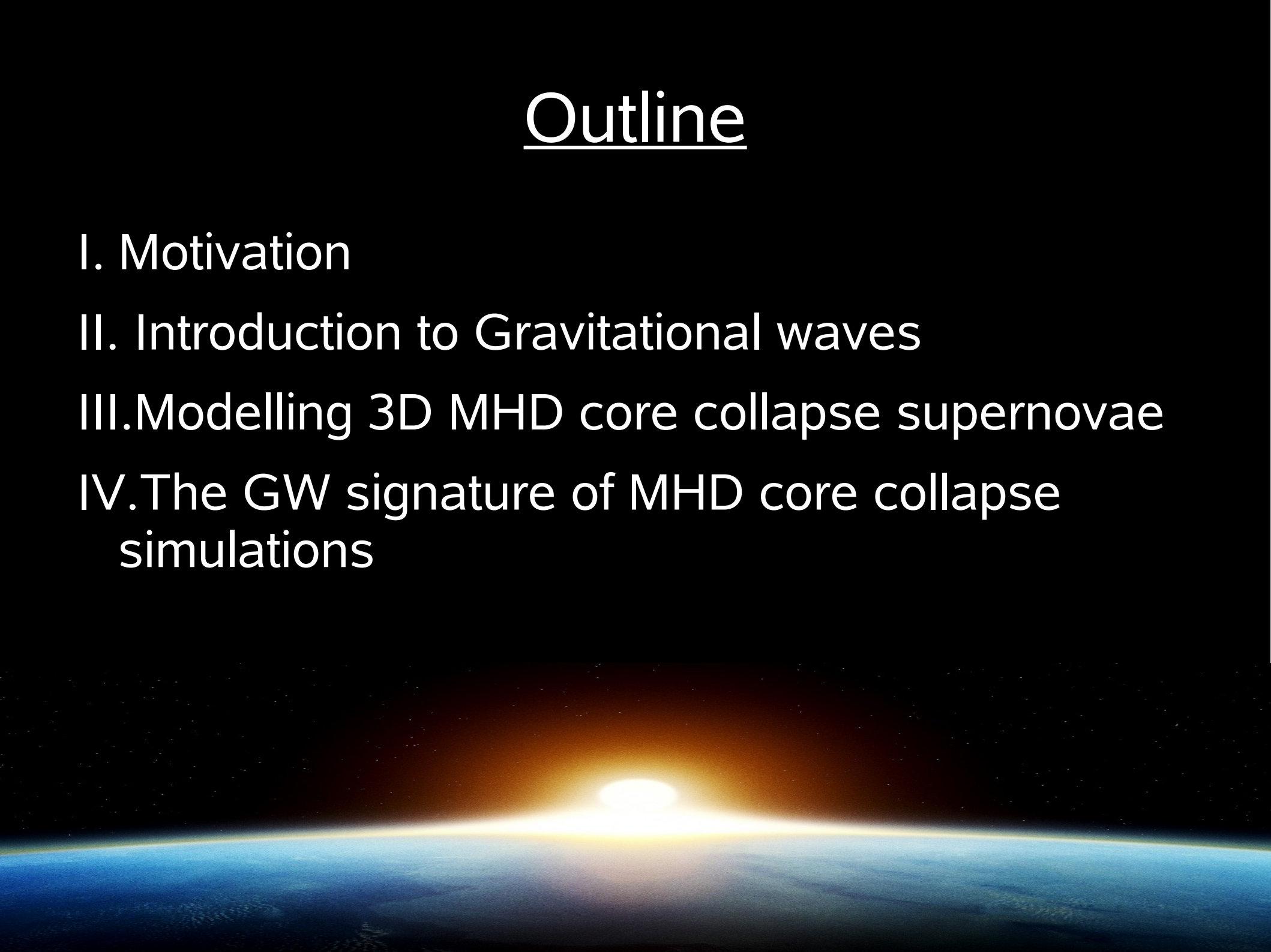

I. Introduction & Motivation

(SN-Mechanism: see e.g. Bethe & Wilson 1995, Buras et al. 2006, Mezzacappa et al. 2006, Marek & Janka 2007, Foglizzo et al 2007, Burrows et al. 2006,...)

- Succesive nuclear burning of a star $M > 8M_{\odot}$ results in an onion skin structure.
- Iron core supported by electron degeneracy pressure until its mass reaches the Chandrasekhar mass.
- Onset of collapse: Photo-dissociation and electron capture.
- The core collapses at supersonic velocities.
- EoS stiffens at $\rho_{nuc} \approx 2 \times 10^{14} [g/cm^3]$

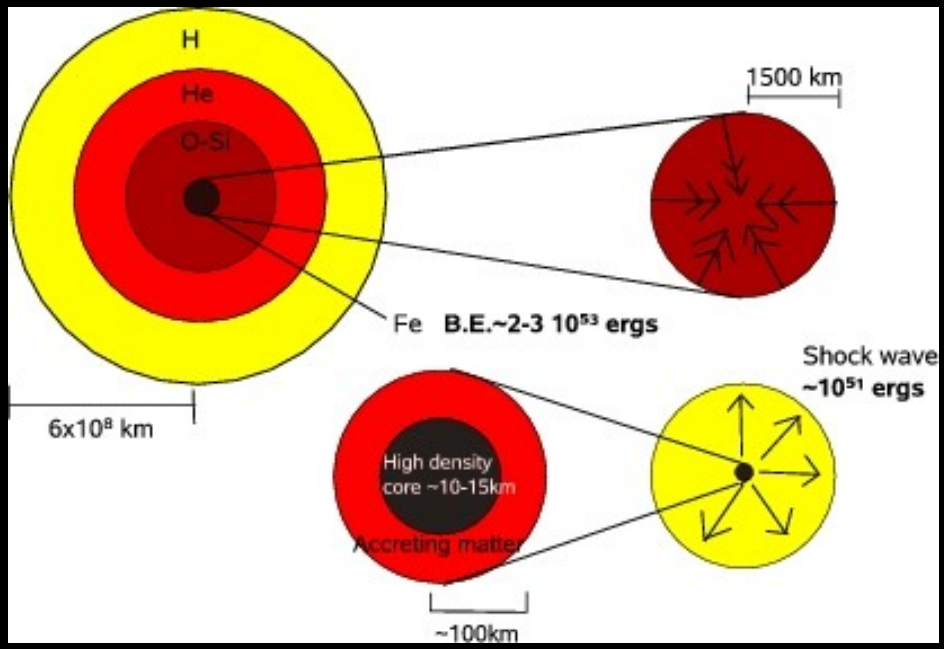

- Inner core bounces back.
- The ratio of the Schwarzschildradius to the radius of the object: for a neutron star this ratio is ~0.3 ->**GR important!**

$$\frac{R_S}{R} = \frac{2GM}{R\,c^2}$$

What can we learn of SNe GWs?

How to constrain SNe mechanism by observations ?

-Electromagnetic radiation. (Optical, X-rays, nuclear decays,...)
-Neutrinos. (Surface of last scatter)
-Gravitational waves (rises from bulk motion of dense concentrations of energy and mass)

Observational input of electromagnetically hidden regions crucial for simulations (both ν & GW). A succesful measurement of GW could in principle provide information about:

- Nuclear physics (Compressiblilty of matter/EoS)
- The explosion mechanism itself.(-> Christian's talk)
- Impose constraints on the nonaxisymmetric SN dynamics in postbounce phase (Convection/ rot. instabilities/ anisotropic ν-emission...)
-...

Binary pulsar PSR 1916 + 13

Figure: from Thorne (1994)

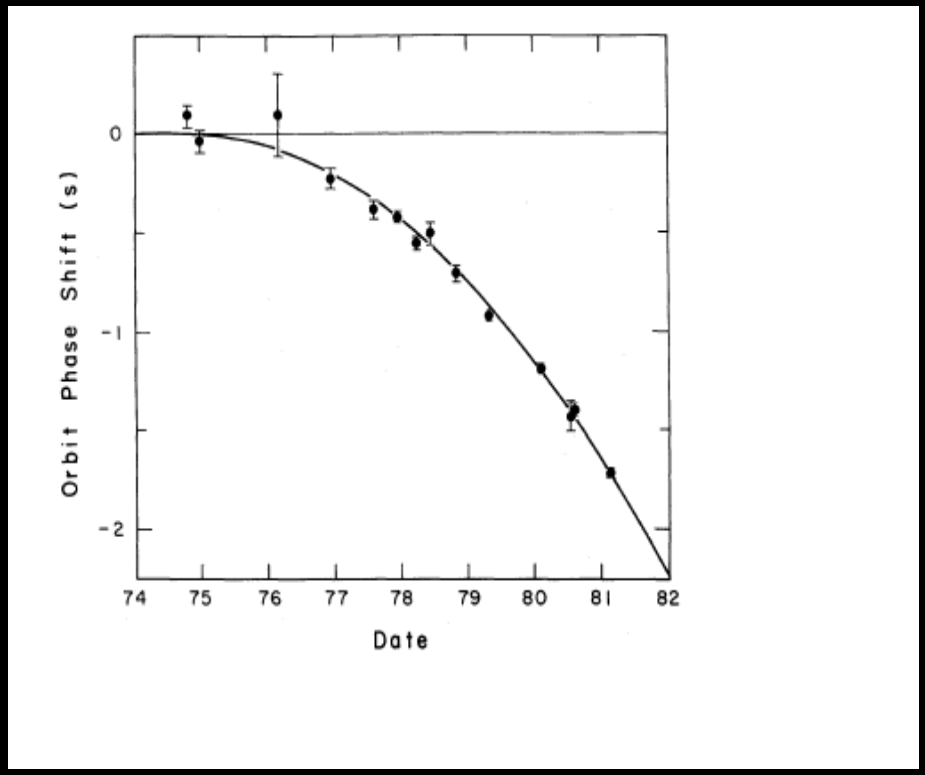

Figure: from Taylor & Weisberg (1982)

Indirect proof of existence: Taylor & Hulse: Nobel prize 1993
Orbital inspiral & energy loss: measured data fit better than 1% to the computed ones.

But: No direct observations of GWs by now!

II. Introduction to Gravitational waves

In Einstein's theory, dynamics of spacetime is governed by the field equations:

$$G_{\alpha\beta} = 8\pi G/c^4 \, T_{\alpha\beta}$$

where the Einstein tensor, $G_{\alpha\beta}$ describes the curvature of spacetime, induced by a stress-energy tensor, $T_{\alpha\beta}$.
The dynamics of matter is governed by the conservation law:

$$T^{\alpha\beta}{}_{;\alpha} = 0$$

The structure of spacetime is described by a metric tensor that can be split into the 3+1 form

$$g_{\alpha\beta} = \begin{pmatrix} g_{tt} & g_{tj} \\ \text{sym.} & \gamma_{ij} \end{pmatrix}$$

where g_{tt} and g_{tj} are kinematical variables, representing the evolution of the coordinate system. There is freedom in choosing them. The real dynamics of the spacetime is entirely contained in the time evolution of the spatial metric γ_{ij}. Thus, after choosing a coordinate system and gauges for the lapse and shift, the time evolution of a spacetime is described by a system of 6 nonlinear equations of the form:

$$\frac{\partial^2}{\partial t^2}\gamma_{ij} = f(g_{\alpha\beta}, T_{\alpha\beta})$$

Linearised theory in a flat background

In the simplest case. one can consider space time dynamics to be a linear perturbation of flat Minkowski spacetime:

$$g_{\alpha\beta} = \eta_{\alpha\beta} + h_{\alpha\beta} \qquad |h_{\alpha\beta}| << 1$$

where $\eta_{\alpha\beta}$ = diag(-1,1,1,1) is the Minkowski metric.

There is a gauge freedom in choosing the coordinate system for linear perturbations.

Make a long story short: 2 physical degrees of freedom, represented by the Transverse Traceless TT-gauge.

Hence, the only non-zero perturbed metric components are:

$$h^{TT}_{xx} = -h^{TT}_{yy} = h_+(t-z)$$
$$h^{TT}_{xy} = h^{TT}_{yx} = h_\times(t-z)$$

There are two possible, independent polarisations h+ and hx, so that one can write

$$h^{TT}_{ij} = h_+ e^{(+)}_{ij} + h_\times e^{(\times)}_{ij}$$

$$e^{(+)}_{ij} = \begin{pmatrix} 0 & 0 & 0 & 0 \\ & 1 & 0 & 0 \\ \text{sym.} & & -1 & 0 \\ & & & 0 \end{pmatrix}$$

$$e^{(\times)}_{ij} = \begin{pmatrix} 0 & 0 & 0 & 0 \\ & 0 & 1 & 0 \\ \text{sym.} & & 0 & 0 \\ & & & 0 \end{pmatrix}$$

Non-vacuum spacetime

If the spacetime is not globally vacuum, one has to solve in priciple the following wave-equation:

$$\Box h_{\alpha\beta} = -16\pi G/c^4 \, T_{\alpha\beta}$$

Analytic solution: Retarded Green's function. Problem: $T_{\alpha\beta}$ in principle contains also quantities arising from the gravitational field.

We have to take further approximations → **Large-distance, slow-motion approximation**
If ***L*** is size of the source and τ is timescale of it's varations, one can assume the following two approximations (see e.g. Misner et al. 1973):

1.) The distance from the source is large: r >> L

2.) The source is slowly-varying, which implies that its internal velocities are small compared to the speed of light.

With these definitions, the gravitational wave solution in the TT-gauge becomes:

$$h_{jk}^{TT}(\vec{x},t) = \frac{2}{r}\frac{G}{c^4}\frac{d^2 \mathbf{t}_{jk}^{TT}(t - r/c)}{d^2 t}$$

with t^{TT}_{jk} being the reduced quadrupole moment, evaluated at a retarted time.
r denotes the distance to the source.

Extracting GWs of SNe

We do not assume any symmetry.
The GW field h_{ij}^{TT} can be resolved into two orthogonal polarisations with amplitudes A+, Ax:

$$h_{ij}^{TT}(\mathbf{X},t) = \frac{1}{R}(A_+ e_+ + A_\times e_\times).$$

R: distance to the source

Unit polarisation tensors in spherical coordinates:

$$\begin{aligned} e_+ &= e_\theta \otimes e_\theta - e_\phi \otimes e_\phi \\ e_\times &= e_\theta \otimes e_\phi + e_\phi \otimes e_\theta . \end{aligned}$$

In the slow motion limit (Misner et al. 1973):
A+ and Ax in first order are given by linear combinations of the second time derivative of the transverse traceless mass quadrupole tensor.

$$\begin{aligned} A_+ &= \ddot{t}_{\theta\theta} - \ddot{t}_{\phi\phi} \\ A_\times &= 2\ddot{t}_{\theta\phi} . \end{aligned}$$

Extracting GW: formalism in use (II)

In the Cartesian orthonormal basis, the quadrupole tensor given by:

$$t_{ij}^{TT} = \frac{G}{c^4}\int dV\rho\left(x_i x_j - \frac{1}{3}\delta_{ij}r^2\right)$$

Shortcuts in the Standard Quadrupole Formula:
Numerical high-frequency noise (Evaluation of 2nd time derivative),
r^2 arm → bad performance of a direct evaluation of the SQF.

Alternative post-Newtonian expressions (Finn & Evans 1990, Blanchet et al. 1990).
First & second order time derivatives of quadrupole moment are transformed into hydrodynamical variables which are known from the core collapse simulation.

$$\dot{t}_{ij}^{TT} = \int dV\rho\left[v_i x_j + v_j x_i - \frac{2}{3}\delta_{ij}(v_1 x_1 + v_2 x_2 + v_3 x_3)\right]$$

'First moment of momentum density formulation' (Finn & Evans 1990)

$$\ddot{t}_{ij}^{TT} = \frac{G}{c^4}\int dV\rho\left(2v_i v_j - x_i\partial_j\Phi - x_j\partial_i\Phi\right)$$

'Stress formulation' (Blanchet et al. 1990)

Extracting GW: formalism in use (III)

The polarisation modes can explicitly gained by a coordinate transformation, e.g. ΘΘ-component:

$$t_{\theta\theta} = t_{ij}^{TT} \frac{\partial x^i}{\partial \theta} \frac{\partial x^j}{\partial \theta}$$

This leads to the following non-vanishing components:

$$\begin{aligned}
t_{\theta\theta} &= (t_{xx}^{TT} \cos^2\phi + t_{yy}^{TT} \sin^2\phi + 2t_{xy}^{TT} \sin\phi\cos\phi)\cos^2\theta \\
&+ t_{zz}^{TT} \sin^2\theta - 2(t_{xz}^{TT} \cos\phi + t_{yz}^{TT} \sin\phi)\sin\theta\cos\theta \\
t_{\phi\phi} &= t_{xx}^{TT} \sin^2\phi + t_{yy}^{TT} \cos^2\phi - 2t_{xy}^{TT} \sin\phi\cos\phi \\
t_{\theta\phi} &= (t_{yy}^{TT} - t_{xx}^{TT})\cos\theta\sin\phi\cos\phi + t_{xy}^{TT} \cos\theta(\cos^2\phi \\
&- \sin^2\phi) + t_{xz}^{TT} \sin\theta\sin\phi - t_{yz}^{TT} \sin\theta\cos\phi.
\end{aligned}$$

For simplicity, we evaluate only the gravitational wave amplitudes for Θ = Φ = 0 (along polar axis; denoted with subscript I), and Θ = π/2, Φ = 0 (equatorial plane, denoted as II)

$$\begin{aligned}
A_{+I} &= \ddot{t}_{xx} - \ddot{t}_{yy} \\
A_{\times I} &= 2\ddot{t}_{xy}
\end{aligned}$$

$$\begin{aligned}
A_{+II} &= \ddot{t}_{zz} - \ddot{t}_{yy} \hat{=} A_{20}^{E2} \\
A_{\times II} &= -2\ddot{t}_{yz}
\end{aligned}$$

Effects of passing GW on particles

- In the TT gauge, the particles do not change coordinate location, i.e the TT gauge represents a coordinate system that is comoving with freely falling particles (Particles that follow geodesics).
- Altough individual particles do not change their coordinate locations in the TT gauge, their proper separation does change.
- Consider two particles on the x-axis, separated by a coordinate distance Lc. The proper separation is:
- Thus, the fractional change in proper separation between the two particles is:

$$\frac{\Delta L}{L_c} \simeq \frac{1}{2} h_{xx}^{TT}$$

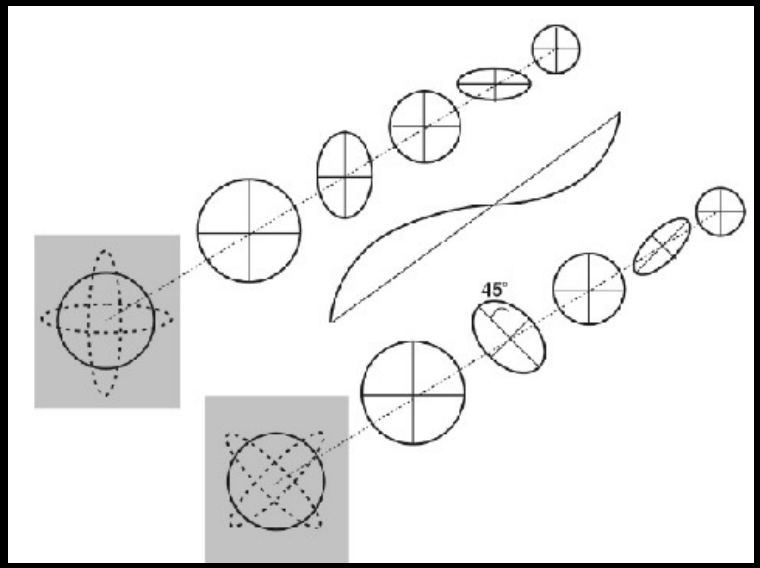

Figure: the effect of the two polarisations (+,x) on a ring of particles. The pol. act similarly, but differ by 45°

$$L = \int_0^{L_c} dx \sqrt{g_{xx}} = \int_0^{L_c} dx \sqrt{1 + h_{xx}^{\rm TT}(t, z=0)}$$
$$\simeq \int_0^{L_c} dx \left[1 + \frac{1}{2} h_{xx}^{\rm TT}(t, z=0)\right] = L_c \left[1 + \frac{1}{2} h_{xx}^{\rm TT}(t, z=0)\right]$$

LIGO (Michelson Interferometer)

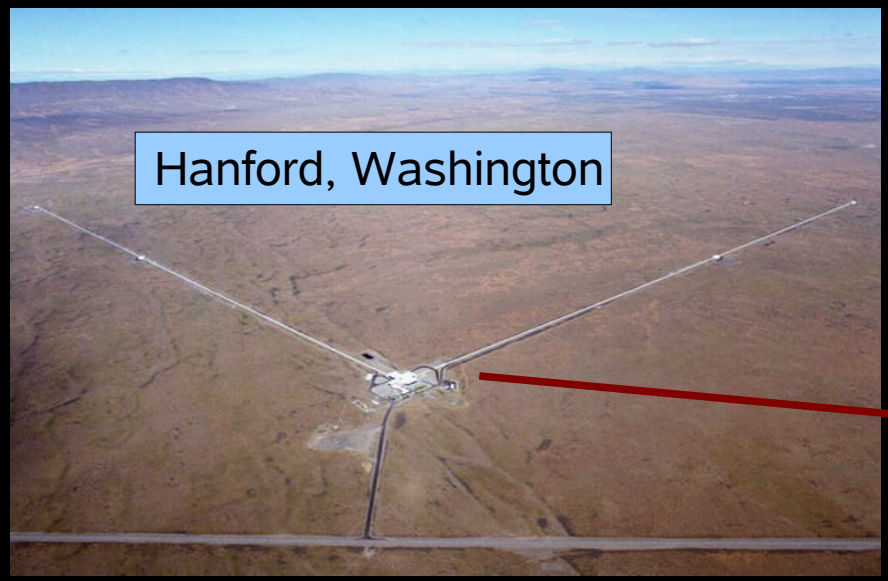

→Measure distance earth-moon at accuracy of several diameters of an atomic nucleus

$$h \hat{=} \frac{\Delta L}{L} \approx 10^{-21} - 10^{-22}$$

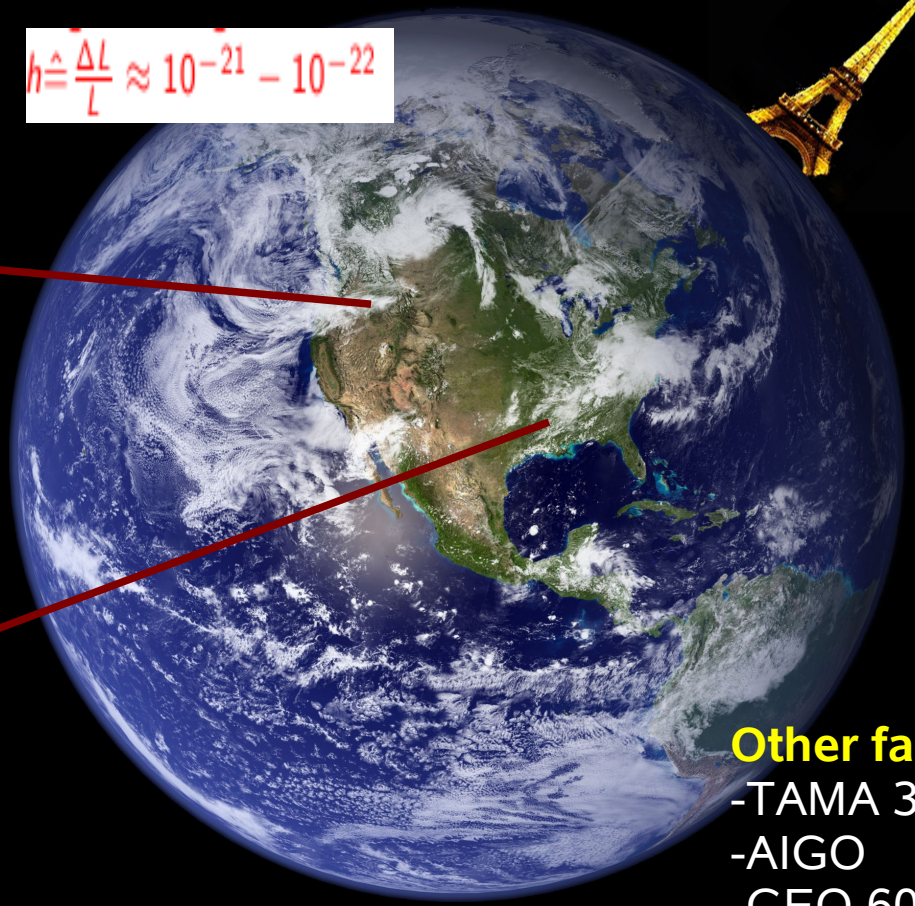

Other facilities:
-TAMA 300
-AIGO
-GEO 600
-VIRGO

LIGO sensitivities

D. Shoemaker (2007), private communication.

- Initial LIGO has three instruments
  Hanford: 4km and one 2km
  Livingston: 4km
- The curves are for a single instrument.
- The curves are for an optimally incident wave in position and polarisation; no averaging over position in given.
- Advanced LIGO has an adjustable frequency response.
  ('nsns' & 'burst' -tuning)
- Limits: seismic, thermal & shot noise.

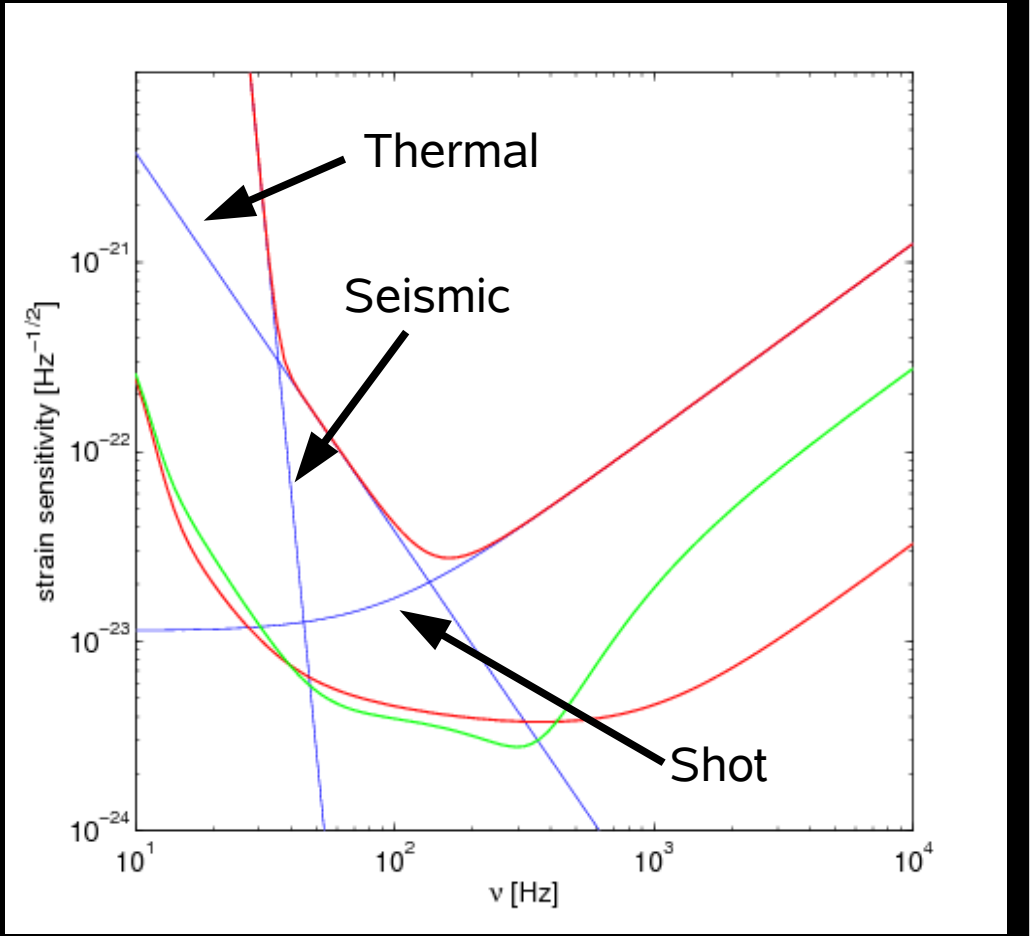

III. Modelling 3D MHD core collapse supernovae

Today: good qualitative agreement about predicted wave-types.
Problem: quantitative predictions sometimes differ strongly due to incomplete input physics.
Robust quantitative GW predictions/templates ultimate goal. Should rely on:

- Well-developed progenitor stars/ templates from stellar evolution.

- Microphysics: Realistic equations-of-state EoS (LS, Shen,...), Neutrino transport/treatment.

- General relativity GR.

-Magnetic fields (MagnetoHydroDynamics - MHD)

- Multi – D effects crucial; 2D, 3D (no generic explosions in 1D, e.g.)
no explosions in 1D (e.g. Liebendörfer et al. 2005,...).

Our hydrodynamical model's input physics – a brief summary (see Roger's & Stuart's talks)

- $15M_{\odot}$ progenitor models at the end of stellar evolution calculations (Woosley & Weaver 1995).
- Hydrodynamics: 3D MHD code (Pen et al. (2003), Liebendörfer et al. 2005/2006).
- Realistic EoS: Lattimer & Swesty 1991
- Gravity: implemented by a spherically symmetric mass integration that includes GR corrections (Marek et al 2006).
- Approximate treatment of neutrino physics (parametrised).
- Central cube of 600^3 km^3 volume; Equidistant Cartesian coordinates. Grid resolution of 1km.
- Central cube embedded in a larger spherically symmetric computational domain, treated by a 1D hydrodynamics code (Liebendörfer et al 2002).

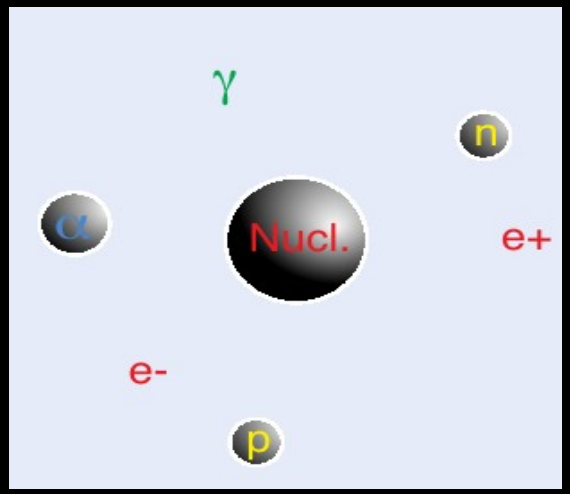

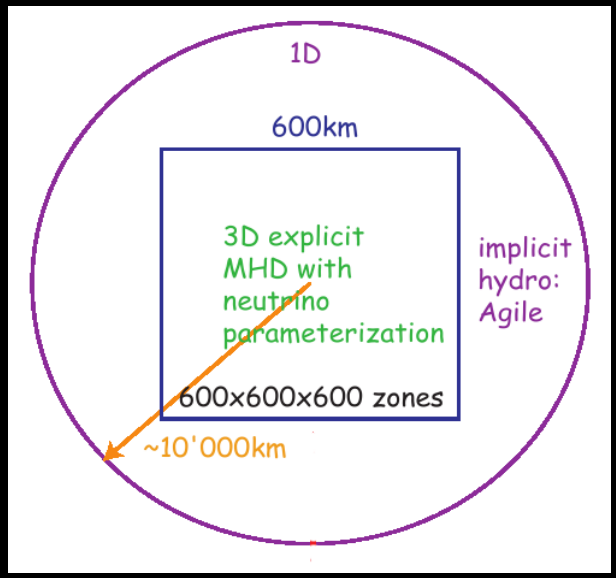

Neutrino physics: parametrised (see Matthias' talk)

- Inclusion of ν-physics in collapse simulations: one major problem.
- Complete Boltzmann ν-transport can only be solved in spherical symmetry (Mezzacappa (2005)) → ν-inclusion either computationally expensive or simplified.
- Neutrino parametrisation scheme:
  → Derived from a tabulation or fit of the electron fraction Ye as a function of density.
- Ye(ρ) only weak function of time.
- Changes in Ye can only be due to electron capture.
  → Possible to deduce changes in entropy and calculate ν-stress from emitted neutrinos.

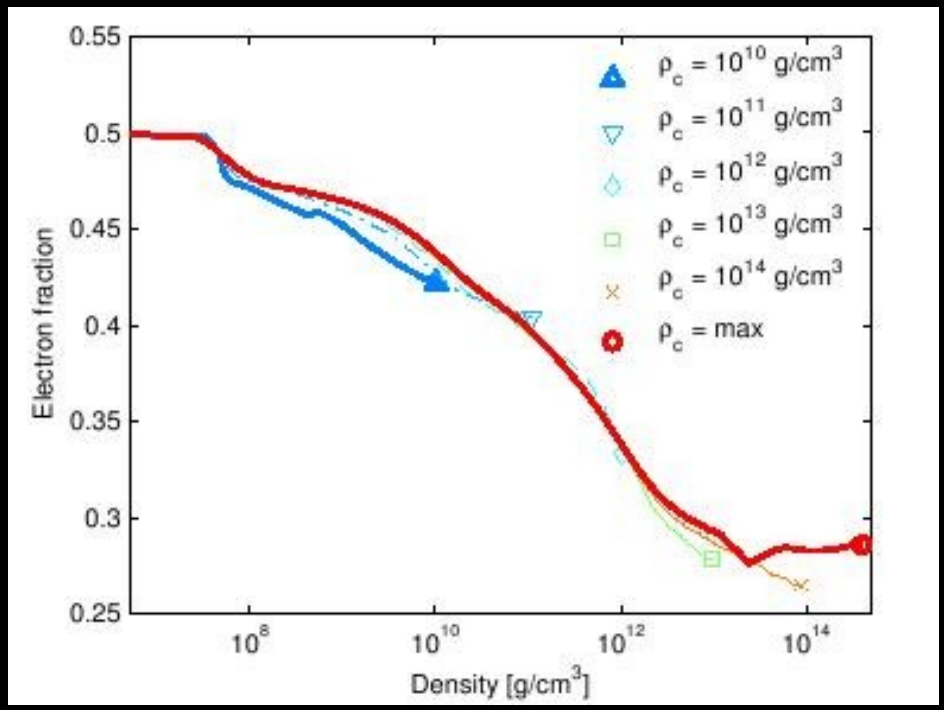

Figure: Electron fraction profiles during core collapse in a spherical symmetric model (Liebendörfer 2005)

Problem: Ye - dip

- Neutrino parametrisation scheme in use is hampered by problems!
- Parametrised ν-scheme cannot model neutrino burst.
- Accretion flows in postbounce phase deleptonize down to Ye ≈ 0.3
  need: Ye ≈ 0.15 → Resulting GW quantitative for times t ~< 5ms.
- Possible solution: spectral ν-diffusion scheme (Liebendörfer et al. (2007); see Stuart's talk)

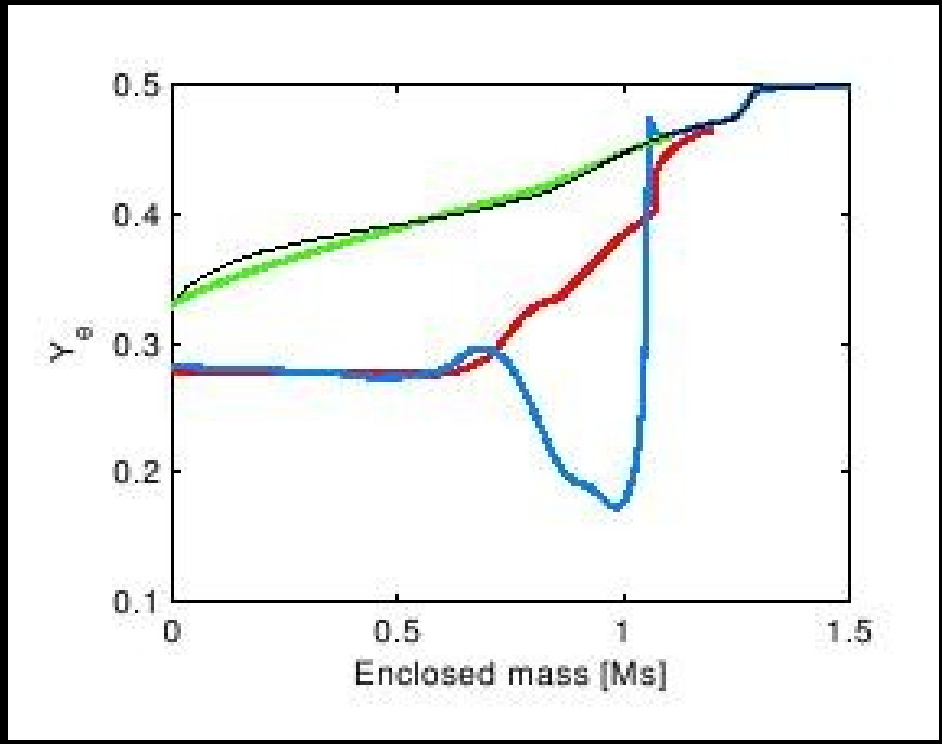

Figure: a nonrotating 3D model compared with a spherically symmetric reference model at different time steps.

Overall speed-up of Code

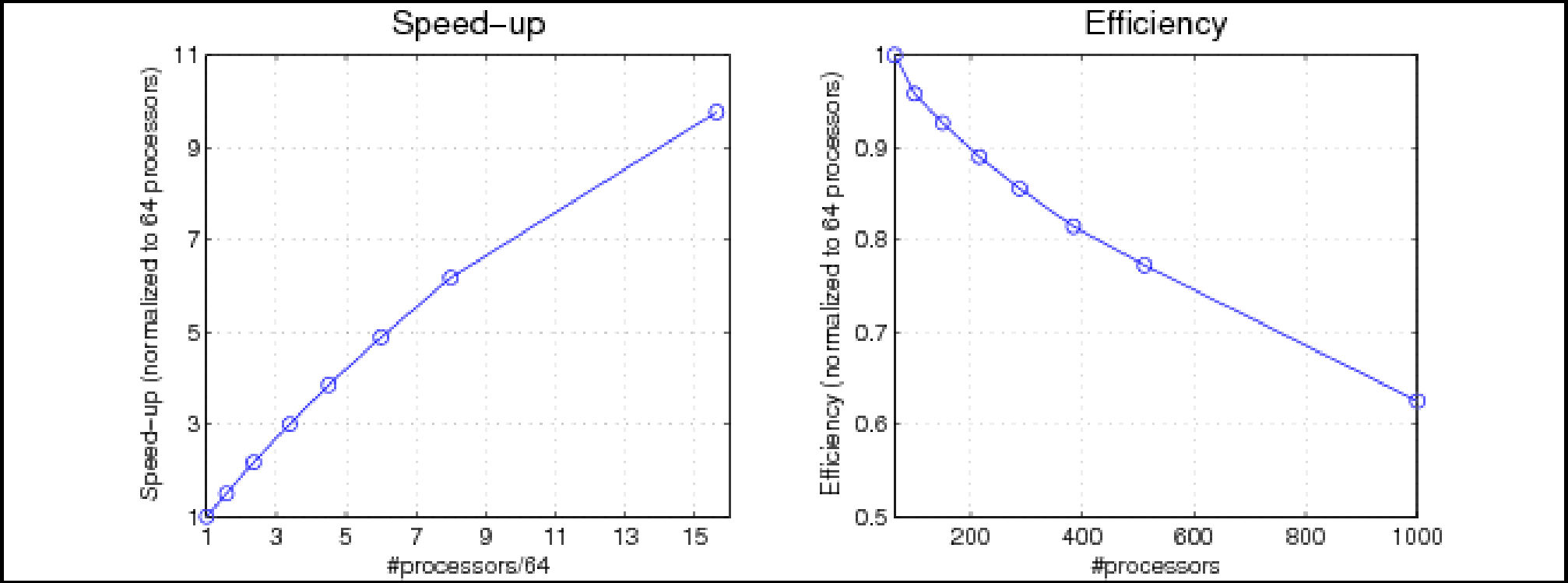

Figure: Speed-up of the used code; tested up to 1000 processors on a CRAY XT3 at the Swiss Supercomputing Centre CSCS. Parallelised by cubic domain decomposition.

IV. The GW signature of MHD core collapse simulations

Visualisation: xy -plane of a rotating core collapse simulation (model s15g).

$\beta_{initial}$ = 0.26%
β_{bounce} = 5.2 %
$B_{poloidal}$ = 1×10^6 [G] (Heger et al. (2005))
$B_{toroidal}$ = 5×10^9 [G]

Swiss Supercomputing Centre
CSCS

GWs from rotating model s15g

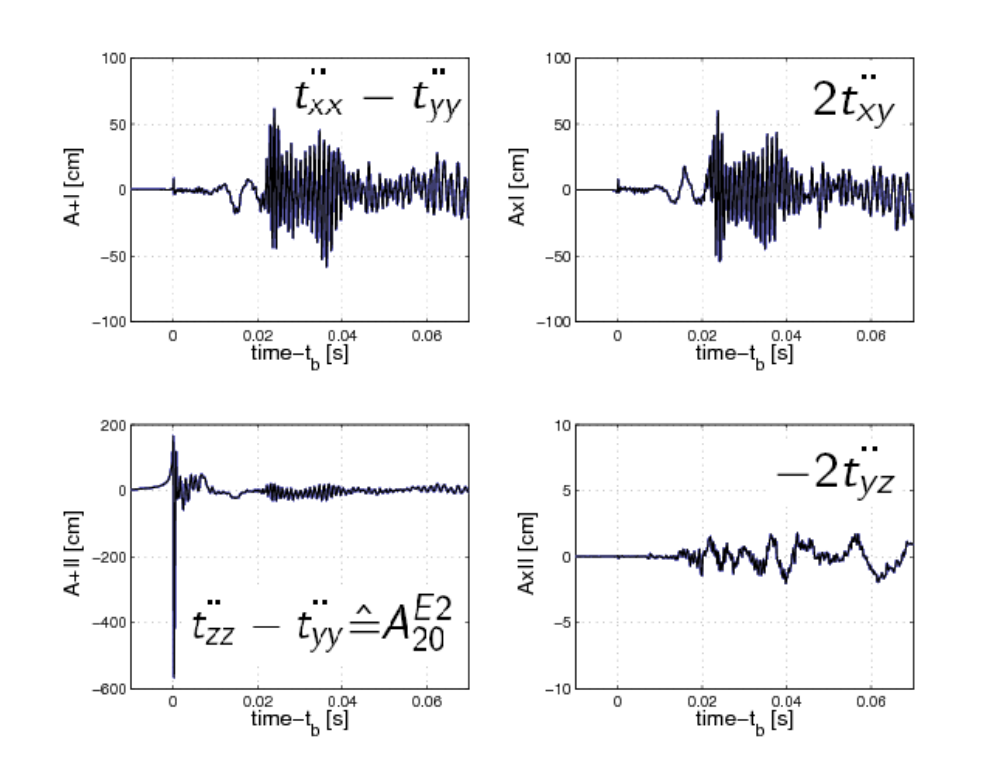

Figure: From Scheidegger et al. 2008.
upper panels: Polar observer +/x; lower panels: Equatorial observer +/x

GW from Rotational core collapse (I)

Early classification until 2007: Three (Four) types of waveforms from core collapse with rotation.
Strong quantitative difference in collapse dynamics and therefore the signal shape.
(e.g. Mönchmeyer et al. 1991, Janka, Zwerger, Mönchmeyer 1993, Zwerger & Müller 1997, Dimmelmeier, Font, Müller 2002,...)

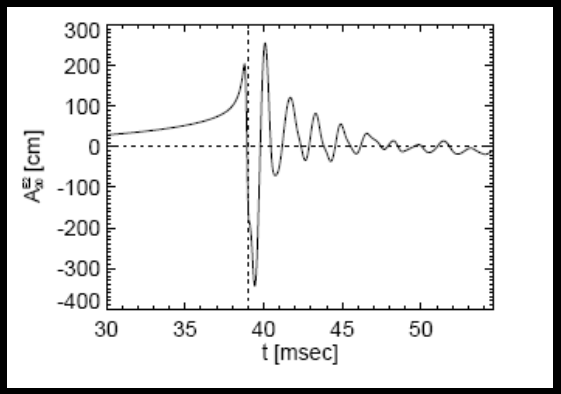

Figure: Type I: Large amplitude at core bounce & damped ring-down oscillations. Core bounce due to the stiffening of the EoS; appears in case of „ordinary“ core collapse. (From Zwerger & Müller 1997)

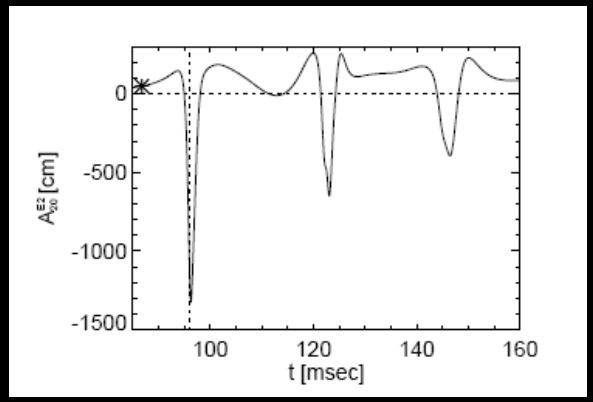

Figure: Type II: Has several distinct peaks, caused by strong centrifugal forces. The core bounces with following coherent re-expansion phases of the inner core. (Zwerger & Müller 1997)

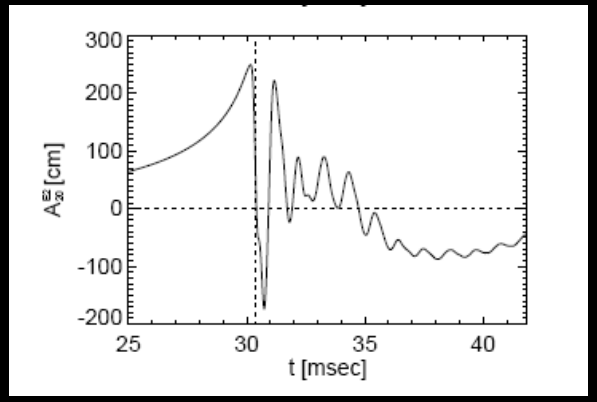

Figure: Type III: „Large“ positive peak at bounce followed by some smaller oscillations with short periods. Appears in case of a fast, pressure-dominated core bounce when the inner core has a very small mass at bounce due to a soft subnuclear EoS or very efficient el.- capture. (Zwerger & Müller 1997)

GW from Rotational core collapse (I)

Early classification until 2007: Three (Four) types of waveforms from core collapse with rotation.
Strong quantitative difference in collapse dynamics and therefore the signal shape.
(e.g. Mönchmeyer et al. 1991, Janka, Zwerger, Mönchmeyer 1993, Zwerger & Müller 1997, Dimmelmeier, Font, Müller 2002,...)

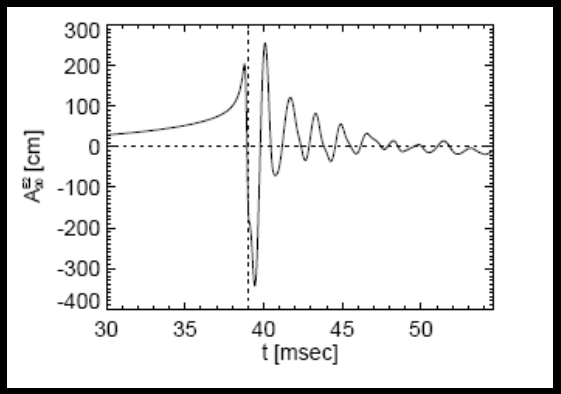

Figure: Type I: Large amplitude at core bounce & damped ring-down oscillations. Core bounce due to the stiffening of the EoS; appears in case of „ordinary“ core collapse. (From Zwerger & Müller 1997)

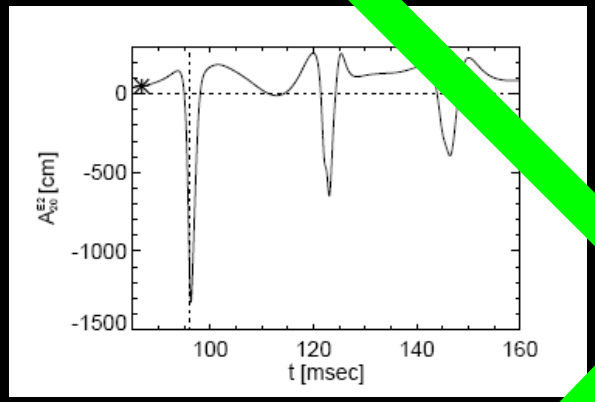

Figure: Type II: Has several distinct peaks, caused by strong centrifugal forces. The core bounces with following coherent re-expansion phases of the inner core. (Zwerger & Müller 1997)

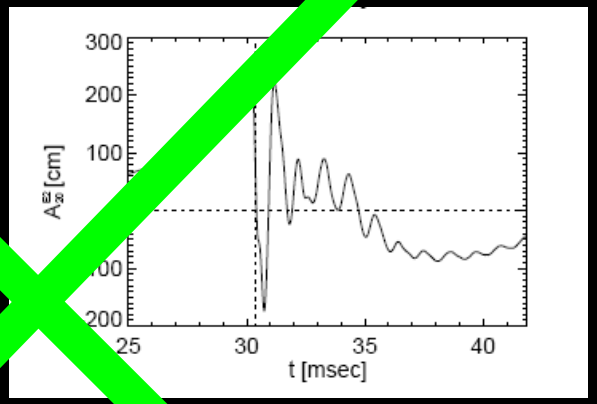

Figure: Type III: „Large“ positive peak at bounce followed by some smaller oscillations with short periods. Appears in case of a fast, pressure-dominated core bounce when the inner core has a very small mass at bounce due to a soft subnuclear EoS or very efficient el.- capture. (Zwerger & Müller 1997)

GW from Rotational core collapse (II)

- Realistic input physics: Only type I (Dimmelmeier et al. 2007; Ott et al. 2007; Dimmelmeier et al. 2008).
- 2D/3D simulations with microphysical EoS, GR & deleptonisation scheme
  →Type I signal generic.
- GR & delept.: lowers the effective adiabatic index.
- Core stays axisymmetric during collapse & early postbounce phase (Only Amplitude A+II large).
- Bounce signal qualitatively weak dependent on rotation rate, progenitor mass, EoS,...
  → Unlikely that bounce signal reveals a lot of information about the original progenitor state.
- Need further GW informations of later SN stages.

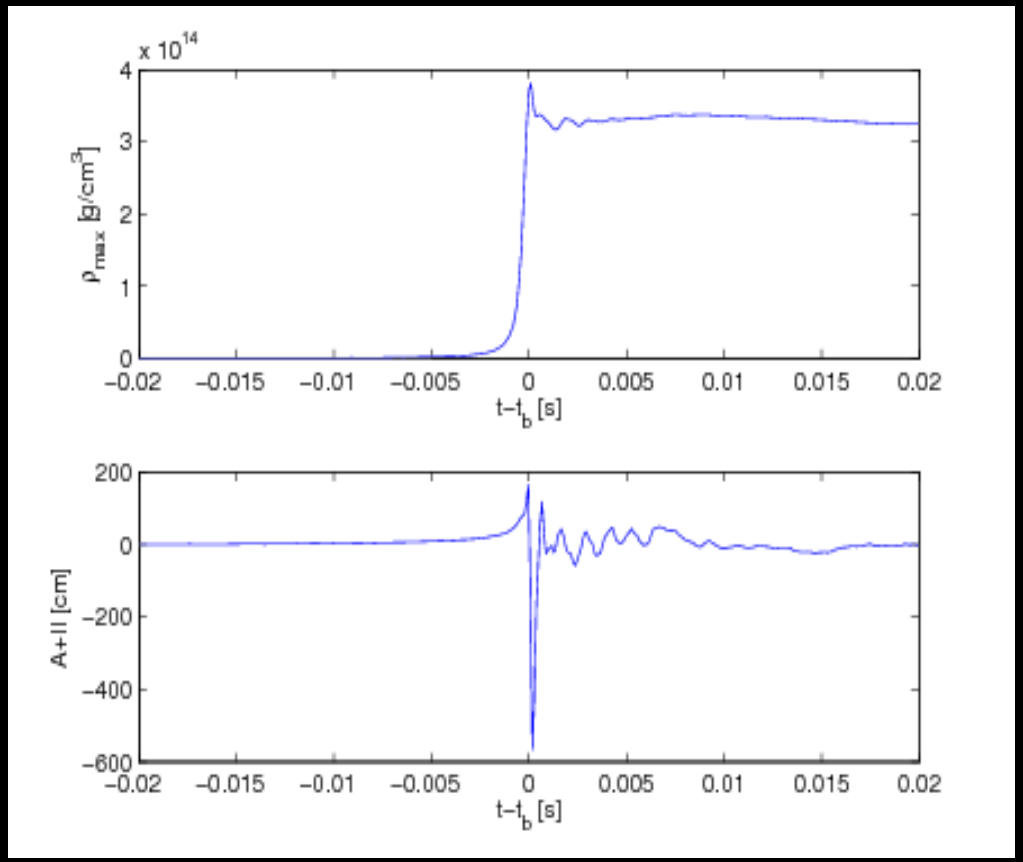

Figure: Time evolution of A+II and density (rotating model s15g)

Low T/|W| rotational instability (I)

(e.g. Saijo et al. 2003, Ott et al. 2005, Watts et al. 2005, Ou & Toholine 2006,Ott et al. 2007, Scheidegger et al. 2008,..)

- Low T/|W| dynamical instability triggered in rotating systems such as neutron stars.
- Pattern speed of unstable mode matches the local angular velocity (Co-rotation point).
- Fig.: dominant m=2 mode
- Contributions from m=1,3.
- Modes m={1,2,3} possess all same pattern speed.
- Narrow band emission at 905 Hz.
- Sudden inset of GW emission triggered as soon as m=2 (bar) mode crosses the m=4 grid background.

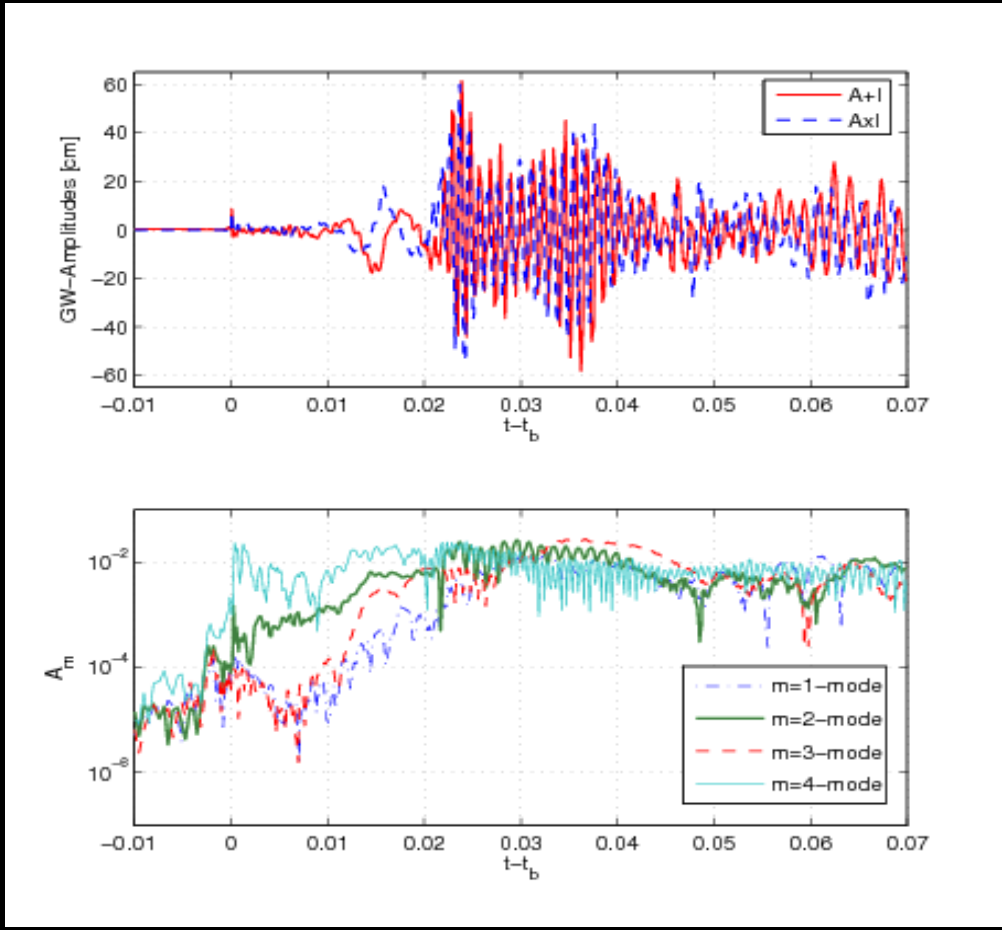

Figure: Upper panel: GW amplitudes A+I, AxI. Lower panel: normalised mode Amplitudes $A_m = |C_m|/C_0$

Low T/|W|-instability - Analysis method:

(See e.g. Watts et al. 2005, Ou & Toholine 2006, Ott et al. 2007)

The analysis method we use to observe the growth of nonaxisymmetric structures decomposes the density at a fixed radius R and constant z-component into its azimuthal Fourier components:

$$\rho(R,z,\phi) = \sum_{m=-\infty}^{\infty} C_m(R,z)e^{im\phi}$$

$$C_m = \frac{1}{2\pi}\int_0^{2\pi} \rho(R,z,\phi)e^{-im\phi}d\phi$$

Normalised mode amplitudes A_m are monitored to measure the growth of unstable modes:

$$A_m = |C_m|/C_0$$

Modes are assumed to behave harmonically as : $\exp[-i(\sigma t - m\phi)]$
where σ is the mode's eigenfrequency.

Pattern speed of m-th mode: $\sigma_p = \sigma/m$

Low T/|W| rotational instability (II)

- GW emission frequency corresponds to the eigenfrequency of the m=2 mode.
- GW polarisations +/x are phase shifted by π/2, as one would expect of a rotating bar.
- No artificial seed perturbations.
- One of the most promising SN features in terms of being detectable.
- In very good agreement with 3D simulations with similar input physics (Ott et al. 2007)
- Low T/|W| instability has much lower threshold than Classical T/|W| instability ($\beta_{dyn} \approx 27\%$).

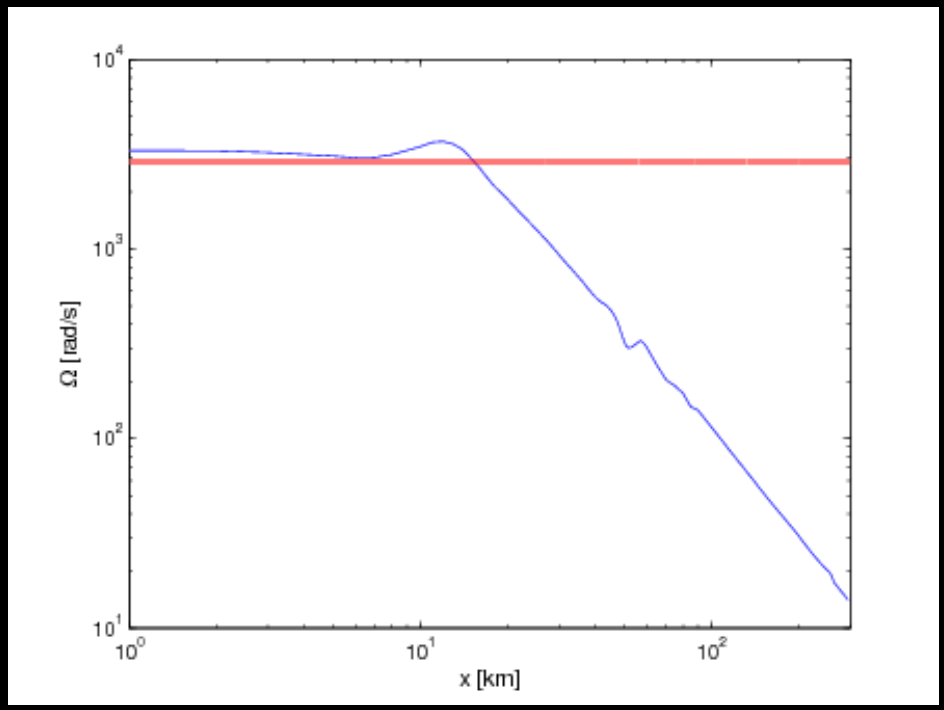

Figure: Angular velocity profile of model s15g vs. pattern speed of the m=2 mode. The innermost 10km are in solid body rotation (quasi-homologous collapse). Corotation point at ≈ 11km.

Comparisons to other simulations

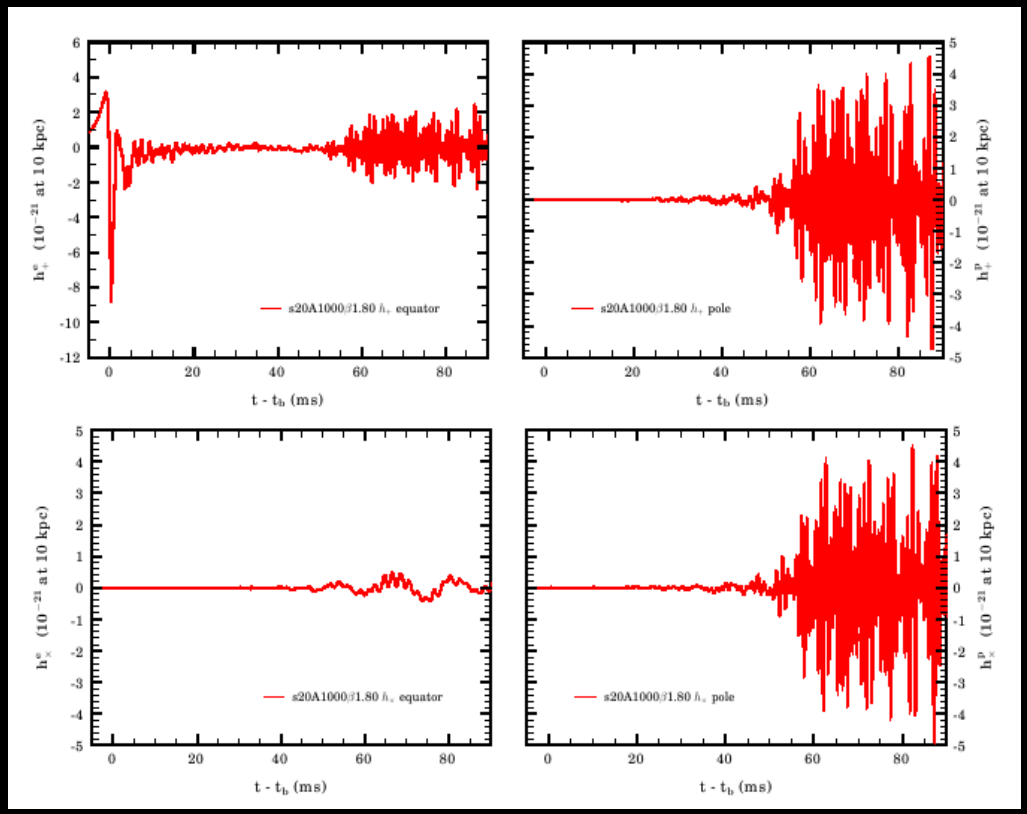

Figure: from PhD C.D. Ott, $20M_\odot$, $\beta_i = 0.37\%$
$f_{GW} \approx 930$ Hz

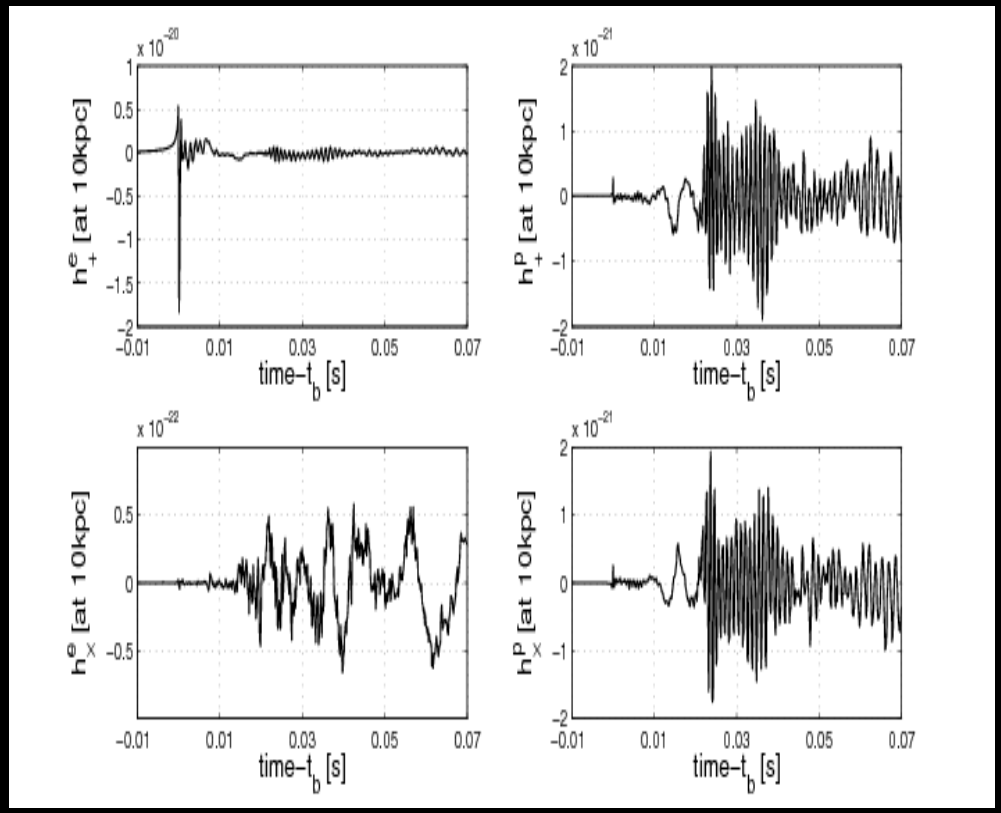

Figure: model s15g, $f_{GW} \approx 905$ Hz,
βinitial = 0.26%

Preliminary results from IDSA

(run performed by S.C. Whitehouse)

- Model v15g
- 2km resolution
- Diffusion: ok
- Heating: no
- $\beta_{initial}$ = 0.26%

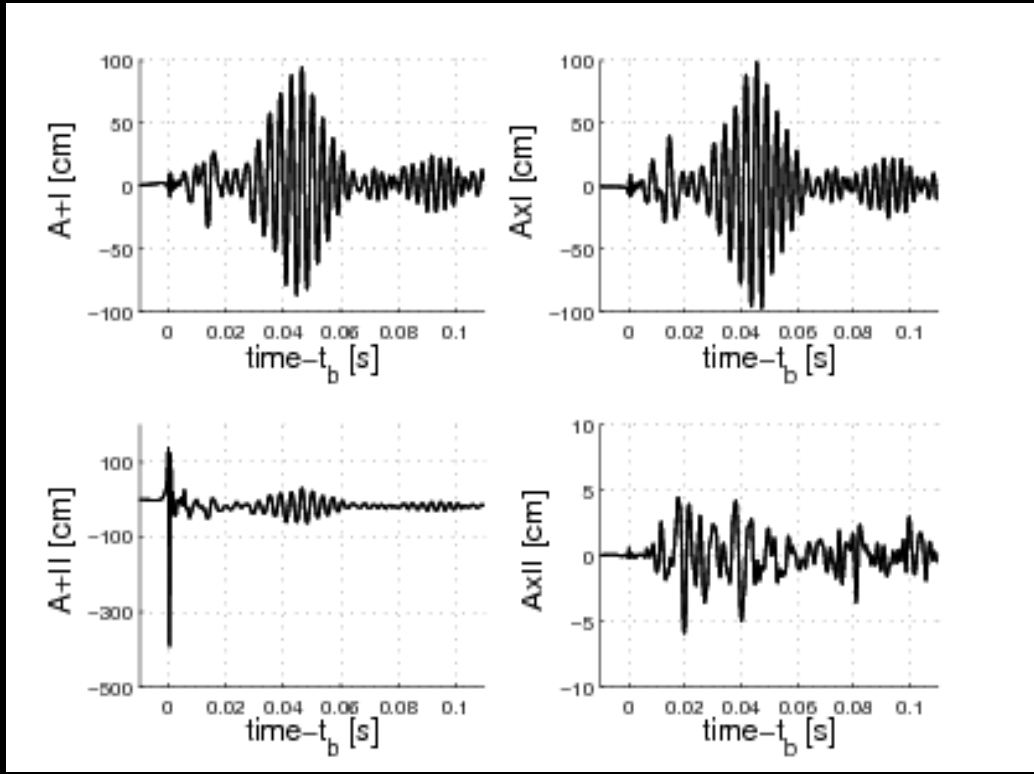

Figure: upper panels: Polar observer +/x; lower panels: Equatorial observer +/x

GWs from (prompt) convection

Movie: xy plane of a quasi nonrotating core collapse simulation (s15h)

- $\beta_{initial} = 0.59 \times 10^{-5}$
- $\beta_{bounce} = 3.1 \times 10^{-4}$
- $B_{poloidal} = 1 \times 10^{6}$ [G] (Heger et al. (2005))
- $B_{toroidal} = 5 \times 10^{9}$ [G]

GWs from Convection (II)

- Induced by negative entropy gradient.
- Low in energy emission.
- Broad-band source.
- Waveforms stochastic, no clear shape or frequency.
- GW emission weak and probably not or only marginally detectable. But: even nonrotating models can develop anisotropic convective instability!

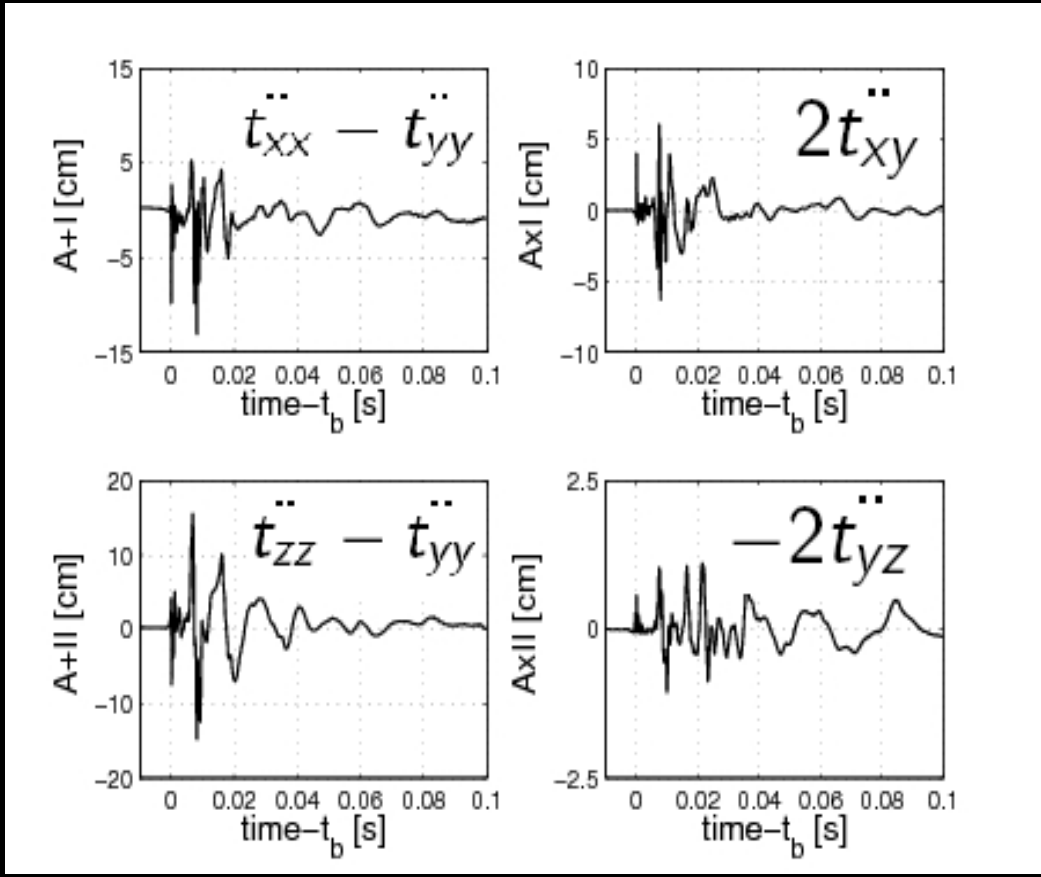

Figure: upper panels: Polar observer +/x; lower panels: Equatorial observer +/x

GW emission & detector sensitivity

- Spectral energy distribution at 10kpc in comparison with the present LIGO/Advanced LIGO (broad band tuning) strain sensitivity.
- Left: rotating model s15g.
- Right: nearly non-rotating s15h.
- Virgo cluster at 15Mpc has event rate of 1/year. Hard at the detector limits, even for Advanced LIGO

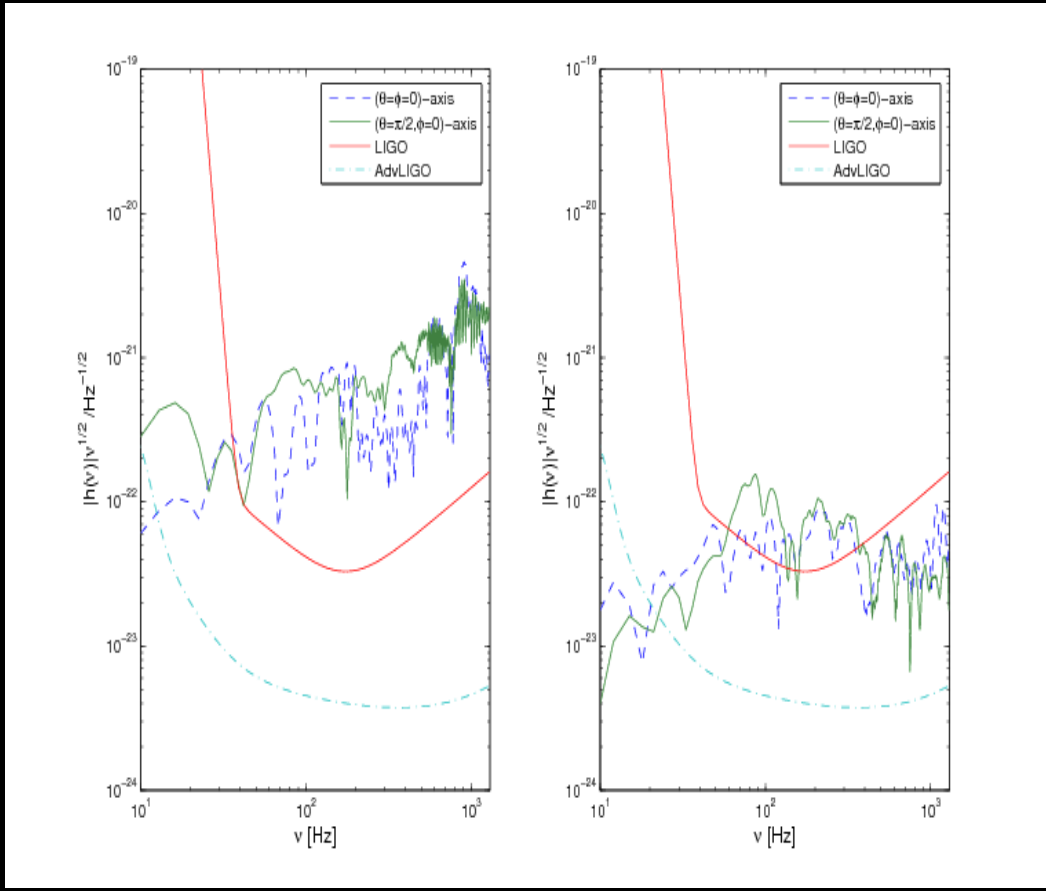

Further remarks

- Weak magnetic fields with $B_{init.tor.} < 10^{11}$G do not change the GW signal (e.g. Kotakte et al. 2004, Obergaulinger et al. 2006, Cerda et al. 2007)
- PNS core oscillations (Ott et al. 2006).
- Anisotropic neutrino emission (e.g. Müller & Janka 1997, Müller et al. 2004, Kotake et al. 2007)
- GW memory effect; marginally detectable (emission at low frequencies)

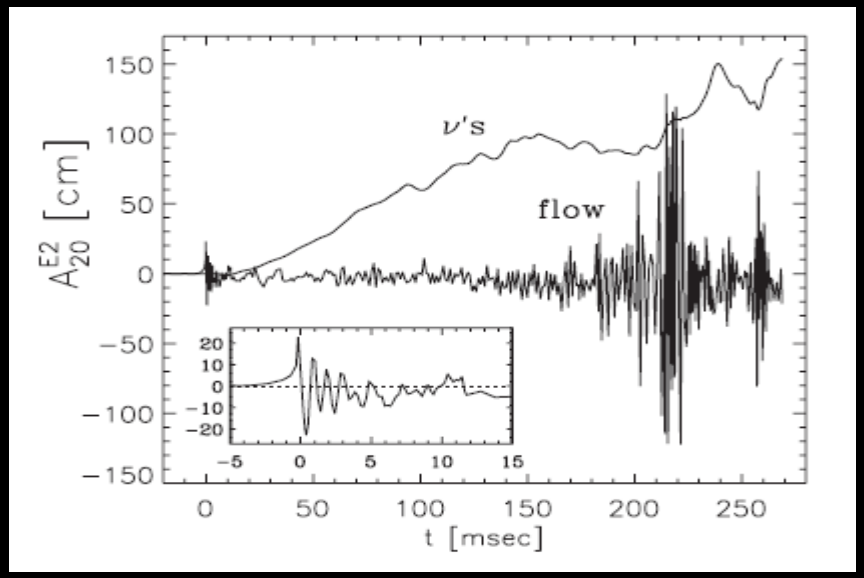

→ More details in Christian's talk...

Figure: 'Burst with memory'-signal (Müller et al. 2004)

Outlook

Upcoming improvements of the code:

- Grid (See Roger's talk)

- IDSA (See Stuart's talk)

- Improved treatment of gravity

Conclusions

Some of the first GW predictions from 3D MHD core collapse SN simulations including „accurate“ microphysics and most important GR features up to the early postbounce phase.

We find type I bounce signals, low T/|W| dynamical instability without adding any artificial seed perturbations and Gws from convection.

In good agreement with simulations using similar input physics, but different numerical schemes.